Z. Phys. C – Particles and Fields 49, 367–374 (1991)

Zeitschrift für Physik C Particles and Fields

Collective characteristics of hadron systems produced in beam fragmentation of $\pi^+ p$ collisions at 250 GeV/c

EHS/NA22 Collaboration

I.V. Ajinenko[8], H. Białkowska[10a], H. Böttcher[2], F. Botterweck[6], F. Crijns[6], A. De Roeck[1b], E.A. De Wolf[1c], K. Dziunikovska[4a], A.M.F. Endler[7], P.F. Ermolov[5], Z.C. Garutchava[9], Y.A. Golubkov[5], N.G. Grigoryan[11], G.R. Gulkanyan[11], P. van Hal[6d], T. Haupt[6e], J.K. Karamyan[11], Z.A. Kirakosyan[11], D. Kisielewska[4a], W. Kittel[6], S.S. Megrabyan[11], F. Meijers[6f], A.B. Michałowska[1], K. Olkiewicz[4a], L.P. Petrovikh[8], A.M. Rybin[8], H. Saarikko[3], L. Scholten[6g], E.K. Shabalina[5], F. Verbeure[1], R. Wischnewski[2], S.A. Zotkin[5]

[1] Universitaire Instelling Antwerpen, B-2610 Wilrijk and Inter-University Institute for High Energies, VUB/ULB, B-1050 Brussels, Belgium
[2] Institut für Hochenergiephysik, O-1615 Berlin-Zeuthen, Federal Republic of Germany
[3] Department of High Energy Physics, Helsinki University, SF-00170 Helsinki, Finland
[4] Institute of Physics and Nuclear Techniques of the Academy of Mining and Metallurgy and Institute of Nuclear Physics, PL-30055 Krakow, Poland
[5] Moscow State University, SU-117234 Moscow, USSR
[6] University of Nijmegen and NIKHEF-H, NL-6525 ED Nijmegen, The Netherlands
[7] Centro Brasileiro de Pesquisas Fisicas, 22290 Rio de Janeiro, Brazil
[8] Institute for High Energy Physics, SU-142284 Serpukhov, USSR
[9] Institute of High Energy Physics of Tbilisi State University, SU-380086 Tbilisi, USSR
[10] University of Warsaw and Institute of Nuclear Problems, PL-00681 Warsaw, Poland
[11] Institute of Physics, SU-375036 Yerevan, USSR

Received 26 September 1990

Abstract. Collective characteristics are studied of hadrons produced in beam fragmentation of non-single-diffractive $\pi^+ p$-interactions at 250 GeV/c. An attempt is made to obtain experimental information on the properties of leading cluster production and fragmentation. On average, the leading cluster carries 0.8 ± 0.1 of the incident momentum, so that the mean value of the inelasticity coefficient of $\langle k \rangle = 0.2 \pm 0.1$ is significantly smaller than that deduced from leading single hadron spectra. The momentum transfer distribution shows that non-single-diffractive processes are less peripheral than diffraction dissociation. The analysis of thrust and sphericity shows jet-like structure of pion fragmentation, that of the charge flow an average forward charge of $\langle Q_f \rangle = 0.45 \pm 0.04$, in agreement with the average charge of the beam valence quarks. Our data are compared to diffraction dissociation and to the Fritiof model.

1 Introduction

According to a number of models of high energy hadron-nucleus collisions, the production of fast particles results from the fragmentation of an excited state (cluster) H^*, which undergoes multiple scatters and then fragments into the final particles outside the nucleus [1–5]. The inclusive spectra of the final state hadrons depend on the properties of H^*, in particular on the inclusive spectra of the process $h p \to H^* X$.

Although excited hadron clusters have been studied extensively in single-diffraction dissociative processes [6–9], almost nothing is known about their properties in non-single-diffractive processes. Information on the latter is important for the understanding of mechanisms of hadron-hadron and hadron-nucleus interactions. Furthermore, it is attractive to compare the features of non-single-diffractive fragmentation with those of single-diffraction dissociation. For the latter a jet-like structure is observed even at our energy [9].

The experimental separation of particles produced in fragmentation of leading clusters from those produced in the central region is a complicated problem and, apparently, one not accurately solvable to the end. Instead of studying a leading cluster fragmenting into a small number of hadrons, one usually restricts oneself to a leading hadron – the fastest product of cluster fragmentation. As a result, the experimental data available on the inelasticity coefficient (part of the incident hadron energy used for production in the central region) represent a distorted picture. In particular, this treatment results in a systematic shift of the inelasticity distribution towards larger values.

In order to obtain more accurate experimental information on the leading cluster spectrum or on the inelasticity distribution, one must detect all fragmentation

[a] Partially supported by grants from CPBP 01.06 and 01.09
[b] Now at MPI, Munich, Germany
[c] Bevoegdverklaard Navorser NFWO, Belgium
[d] Now with Ericsson Telecommunicatie B.V., Rijen, The Netherlands
[e] Now at University of Syracuse, Syracuse, NY, USA
[f] Now at CERN, Geneva, Switzerland
[g] Now with PANDATA, Rijswijk, The Netherlands

products (or at least the energetic ones) including neutral particles. Such an opportunity is provided by the European Hybrid Spectrometer [10, 11] at the CERN SPS. It consists of an active vertex detector (Rapid Cycling Bubble Chamber) embedded in a 2 T magnetic field and a down-stream spectrometer. The spectrometer consists of one wire and six drift chambers and an additional 1 T magnet. The charged particle momenta are measured over the whole solid angle with a resolution ranging from $\langle \Delta p/p \rangle$ of 2.5% at 30 GeV/c to 1.5% above 100 GeV/c [12].

Neutral pions are detected by two electromagnetic calorimeters. The combined acceptance of gamma detectors allows to measure π^0's for $x(\pi^0) \geqq 0.025$ [13]. Part of the remaining gammas and of the short-lived neutral particles are detected and measured within the vertex detector [14].

The data selection and the methods applied to enrich the sample with leading cluster fragmentation are described in Sect. 2. Results are given in Sect. 3 and compared to model predictions in Sect. 4. The conclusions are summarized in Sect. 5.

2 Data selection

The data presented here originate from the NA22 experiment performed with EHS exposed to a meson enriched beam of lab momentum $p_{\text{lab}} = 250$ GeV/c. We accept $\pi^+ p$ events for which the measured and reconstructed charge multiplicities are consistent, charge balance is exactly satisfied, no electron is detected and all tracks are properly reconstructed (see [12]). We require tracks to have a momentum resolution $\Delta p/p < 0.1$ in the forward c.m. hemisphere, but no restriction is imposed on $\Delta p/p$ in the backward hemisphere. Elastic scattering and single-diffraction dissociation events (with $n \leqq 6$) are excluded according to the methods described in [12]. The total number of remaining events is 59131.

Furthermore, to avoid loss of fast neutral particles in the beam fragmentation region, we select events with acceptable total momentum balance. To achieve this, we firstly accept events for which the total longitudinal momentum $p_{\parallel}^{\text{RCBC}}$ of all charged and neutral particles detected in RCBC is within the interval $245 \leqq p_{\parallel}^{\text{RCBC}} \leqq 255$ GeV/c and the total transverse momentum p_T^{RCBC} is less than 0.5 GeV/c. Secondly, if $p_{\parallel}^{\text{RCBC}}$ is less than 245 GeV/c, we add to it the total longitudinal momentum $p_{\parallel}^{\text{EM}}$ of γ's or π^0's and η's reconstructed in the electromagnetic calorimeters, and accept events with total longitudinal momentum within the interval $225 \leqq p_{\parallel}^{\text{RCBC}} + p_{\parallel}^{\text{EM}} \leqq 255$ GeV/c and total transverse momentum $|\mathbf{p}_T^{\text{RCBC}} + \mathbf{p}_T^{\text{EM}}|$ less than 0.5 GeV/c. This allows a loss of no more than 10% of the total momentum and does not significantly affect the characteristics of hadrons in the beam fragmentation region. After this selection, the final data sample comprises 11954 events. Each event is weighted to correct for losses due to selection criteria and interaction trigger efficiency, so that the charge multiplicity distribution of accepted events corresponds to the topological cross section of the non-diffractive $\pi^+ p$ sample [9, 11].

The following step is to select particles actually arising from beam fragmentation. This is by far the most difficult step, since no clear boundary exists between particles produced in beam fragmentation and central production. Any method applied can only be considered to produce a sample *enriched* in beam fragmentation. To obtain a feeling for the degree of stability of the results with respect to the choice of the method, three different methods are compared and the cut parameters of each are varied over reasonable values.

According to the *first method* (the cut method), a selection $y > y_{\text{cut}}$ is applied to the rapidity of each particle. From the range of forward-backward correlations in our data [15] and the size of the scaling region [12], we deduce that at our energy the "optimal" value of y_{cut} is in the interval $1 \leqq y_{\text{cut}} \leqq 2$ (in the c.m.s.). In the tables we present results for $y_{\text{cut}} = 1$ and 2, while the distributions for $y_{\text{cut}} = 1.5$ are presented in the figures. As an alternative to y_{cut}, a Feynman-x cut varied over the range $0.05 \leqq x_{\text{cut}} \leqq 0.15$ has been tried with very similar results.

According to the *second method* (the maximum rapidity gap method), a "boundary" $y_0 > 0$ is determined separately for each event by the maximum rapidity gap $(\Delta y)_{\max}$ between neighbouring particles. If $(\Delta y)_{\max}$ is reached between the k-th and $(k+1)$-th particles ($y_k > y_{k+1}$), we set $y_0 = y_k$ and assume all particles with $y \geqq y_0$ to belong to the beam fragmentation region. (Note, if the largest gap includes $y = 0$, all particles in the forward hemisphere are accepted). Two variants of this method are used: a) no restriction on the $(\Delta y)_{\max}$, b) a restriction $(\Delta y)_{\max} \geqq 1$ is used and events with $(\Delta y)_{\max} < 1$ are rejected. This latter cut reduces the number of events to 10730.

According to the *third method* (the cluster rapidity method), we assume that the difference between the leading cluster rapidity Y_c and the nearest particle not belonging to the cluster exceeds some minimum value ΔY_c, where $\Delta Y_c \approx 1.5$–2. If the rapidity difference between the fastest particle and the nearest one exceeds ΔY_c, only one (the fastest) particle is assumed to be in the beam fragmentation region. If not, the fastest particle is combined, one after the other, with the neighbouring particles, until the composed system (cluster) rapidity Y_c exceeds the nearest particle rapidity by the value of ΔY_c. We, furthermore, require the last particle included into a cluster to have $y > 0.5$. If this requirement is not satisfied the event is rejected. The number of events selected by this method is 7567.

As already stated above, all these methods have draw-backs and can only be considered as methods to *enrich* the selected sample by excited hadron state clusters. In the following we shall compare the three methods, in order to detect possible common trends.

To see the effect of the cuts described above and to be able to compare our experimental results to model predictions, the same cuts are applied to Monte Carlo events generated according to the Lund [16] and Fritiof [17] models.

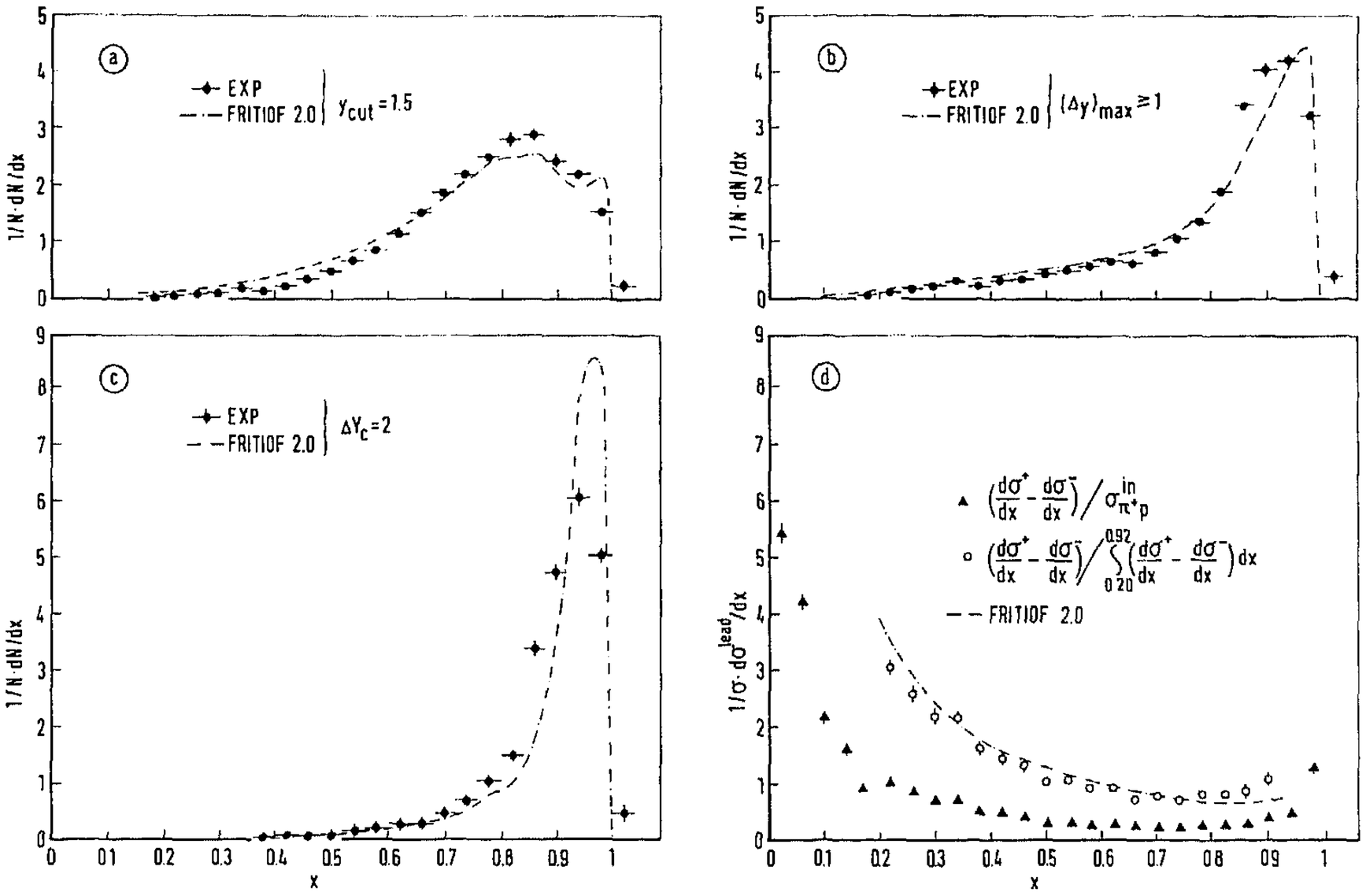

Fig. 1a–d. The X distribution of the leading hadron cluster, for the three different methods of cluster separation: **a** the cut method ($y_{cut}=1.5$), **b** the maximum rapidity gap method ($(\Delta y)_{max}\geqq 1$), **c** the cluster rapidity method ($\Delta Y_c=2$). **d** The x distribution of the leading hadron in $\pi^+ p$ interactions [12], normalized in two different ways. Also the Fritiof 2.0 model predictions are presented

3 Experimental results

The methods described in Sect. 2 are applied for the selection of hadrons to be considered products of non-single-diffractive beam (or leading hadron cluster) fragmentation. The following collective characteristics of the leading hadron cluster are considered:

a) the total longitudinal momentum $P_\parallel$ (both in c.m.s. and lab. frames) or the Feynman variable $X=P^*_\parallel/P^*_{max}$ (Fig. 1a–c), the latter being equal to the "elasticity" coefficient;
b) the squared transverse momentum P_T^2 (Fig. 2);
c) the squared effective mass M^2_{eff} (Fig. 3);
d) the squared four-momentum transfer t from the incident π^+ to the leading hadron system (Fig. 4);
e) the charge multiplicity n_{ch} (Fig. 5), as well as the M_{eff}-dependence of its average, $\langle n_{ch}(M_{eff})\rangle$ (Fig. 6);
f) the charge Q (Fig. 7);
g) the parameters characterizing the possible jet-like structure of leading cluster fragmentation, e.g. thrust T (Fig. 8) and sphericity S, thrust and sphericity angles θ_T and θ_S;

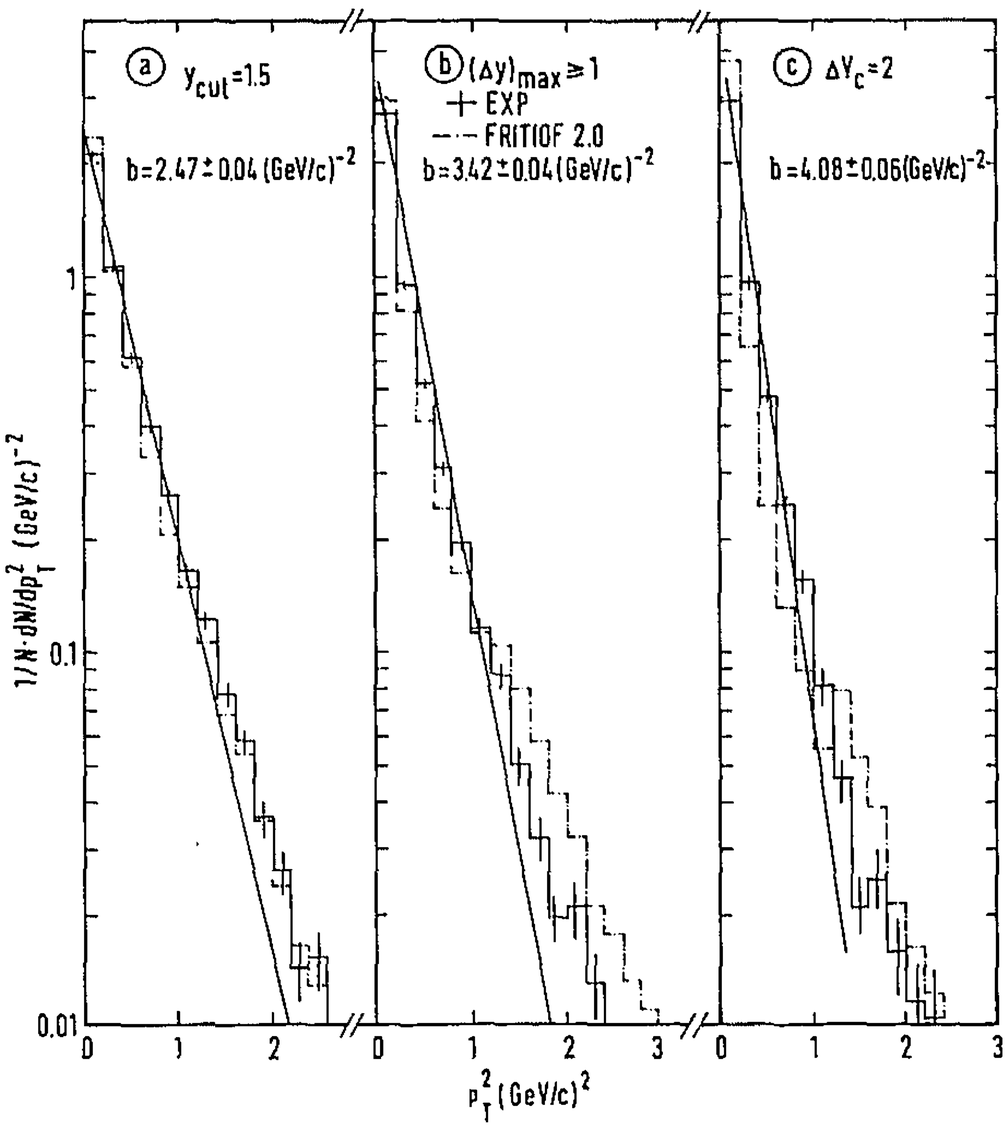

Fig. 2a–c. The P_T^2-distribution of the leading cluster. Results of exponential fits are given by solid lines

From the experimental distributions presented in Figs. 1–8 and from the mean values given in Tables 1 and 2, one can deduce the following trends common to all three selection methods:

1) The Feynman-x distribution of Fig. 1 (and therefore also the $p_\parallel$ distribution) strongly differs from a constant distribution. For all three methods used, the average fraction of incident longitudinal momentum carried by fragmentation products, i.e. the average "elasticity" coefficient, lies in the range $\langle X\rangle=0.8\pm0.1$ (both in c.m. and lab. frames) and the mean inelasticity (part of the incident hadron momentum used for particle production in the central region) is $\langle k\rangle\approx(1-\langle X\rangle)\approx(0.2\pm0.1)$.

One should emphasize that for all three selection methods the X-distribution of the leading cluster strongly differs from the leading hadron spectrum shown in Fig. 1d. When extracting the latter from the NA 22 data

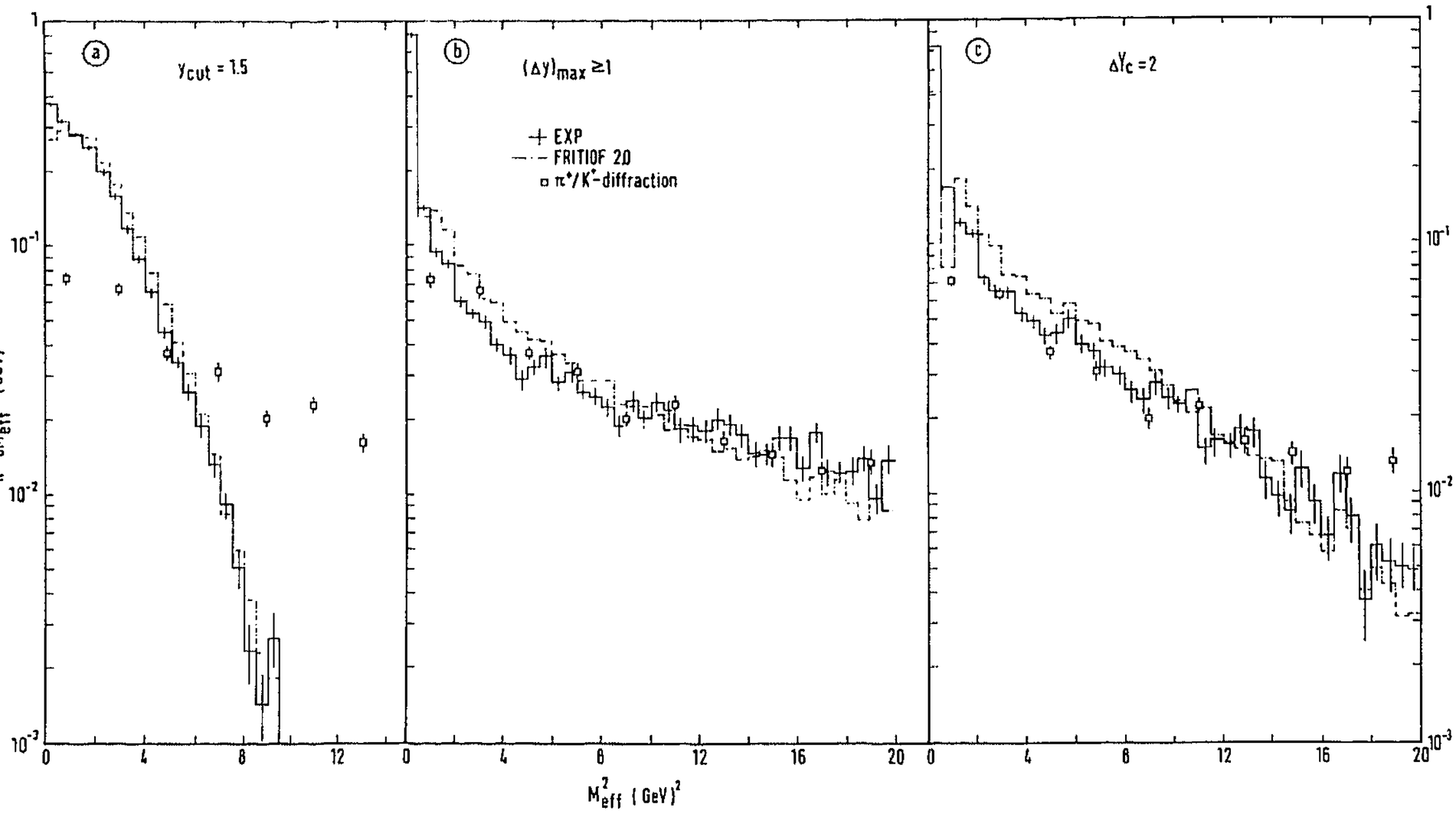

Fig. 3a–c. The effective mass square M^2_{eff}-distribution. The data on π^+/K^+-diffraction at 250 GeV/c [9] are also presented

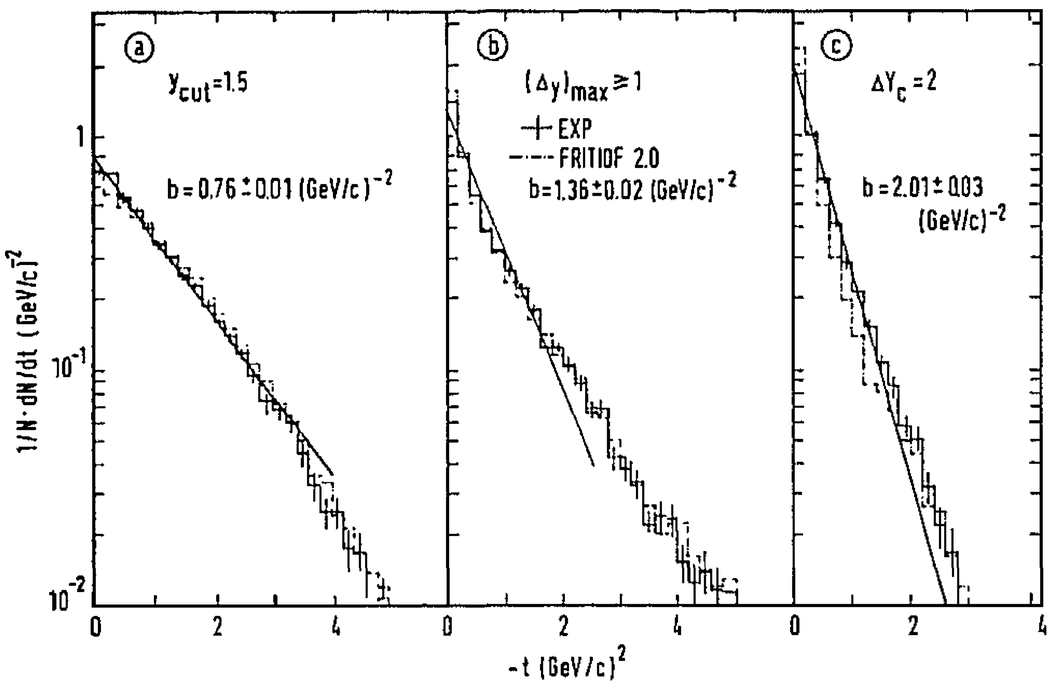

Fig. 4a–c. The t-distribution of the leading cluster. Results of exponential fits are given by solid lines

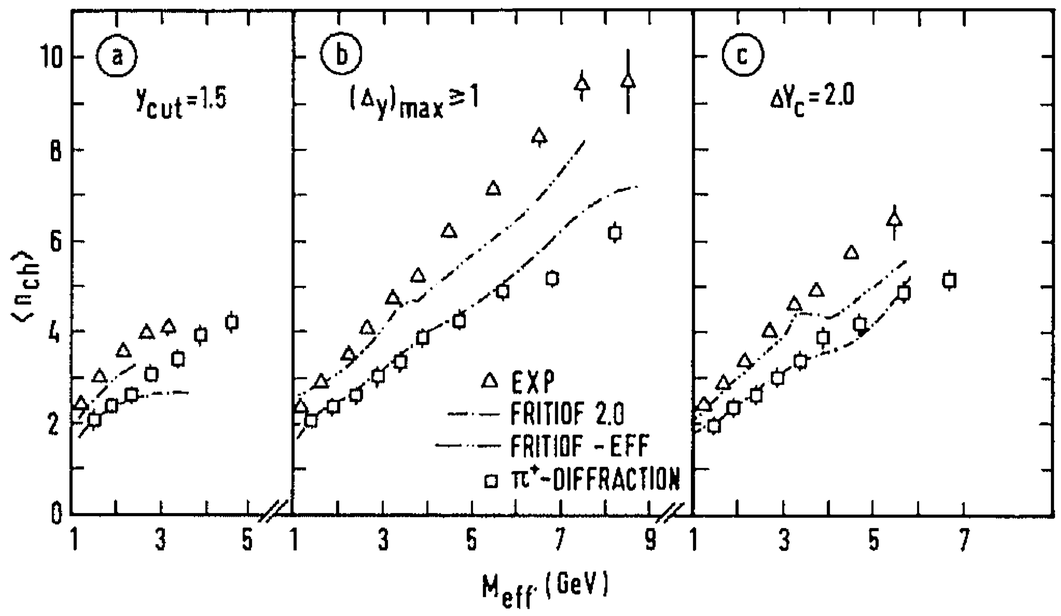

Fig. 6a–c. The M_{eff}-dependence of the mean charge multiplicity $\langle n_{ch} \rangle$ of the leading cluster. The data on π^+/K^+-diffraction at 250 GeV/c [9] are also presented

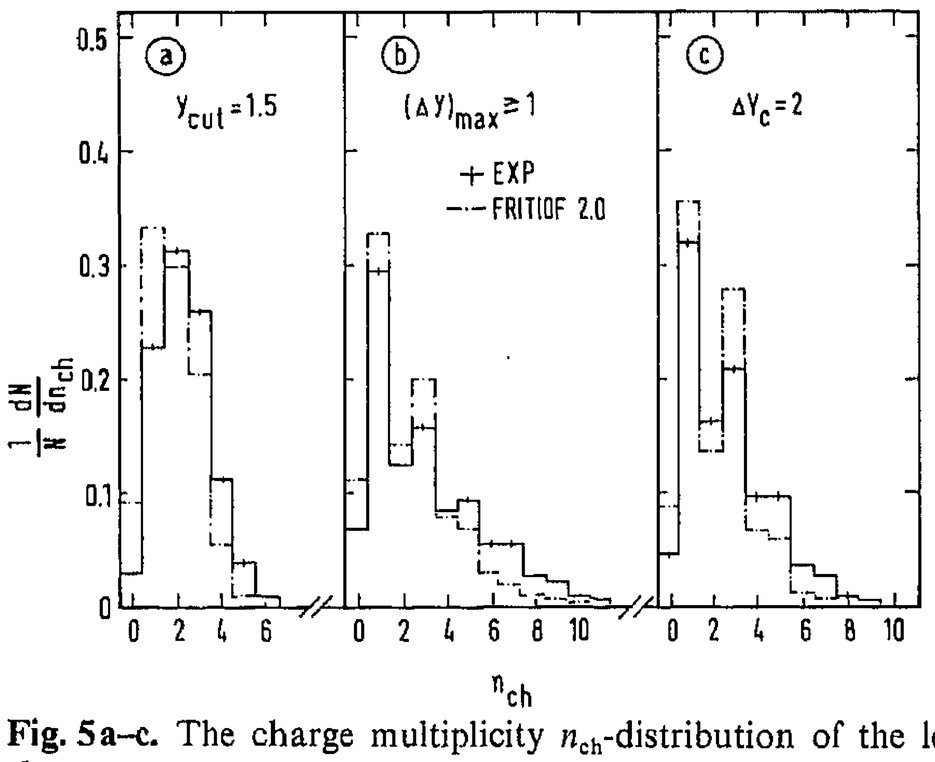

Fig. 5a–c. The charge multiplicity n_{ch}-distribution of the leading cluster

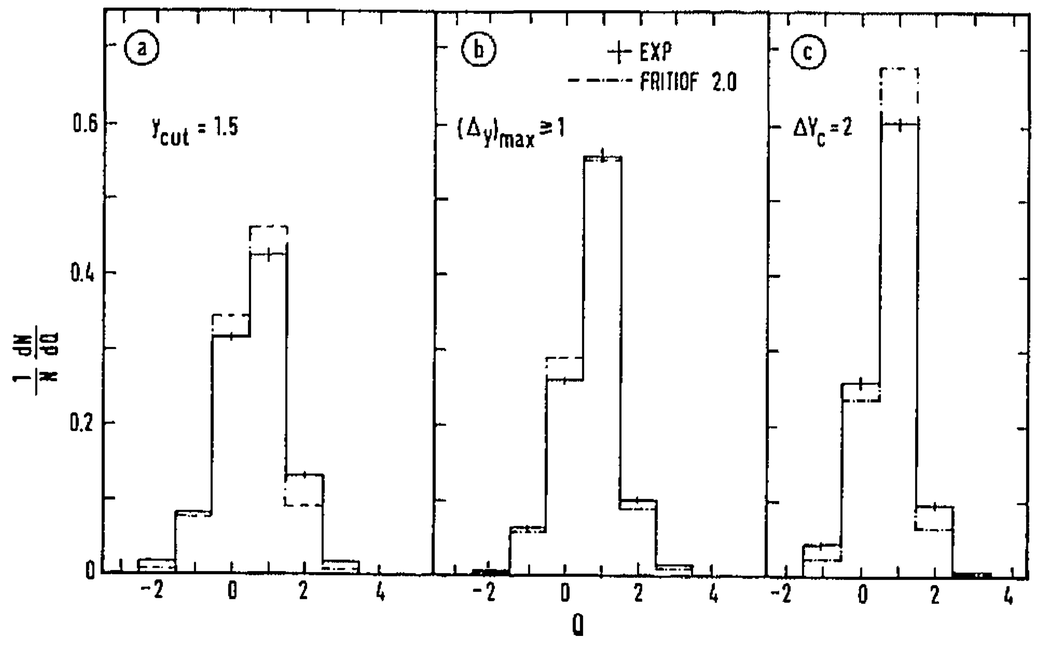

Fig. 7a–c. The summed charge Q-distribution of the leading cluster

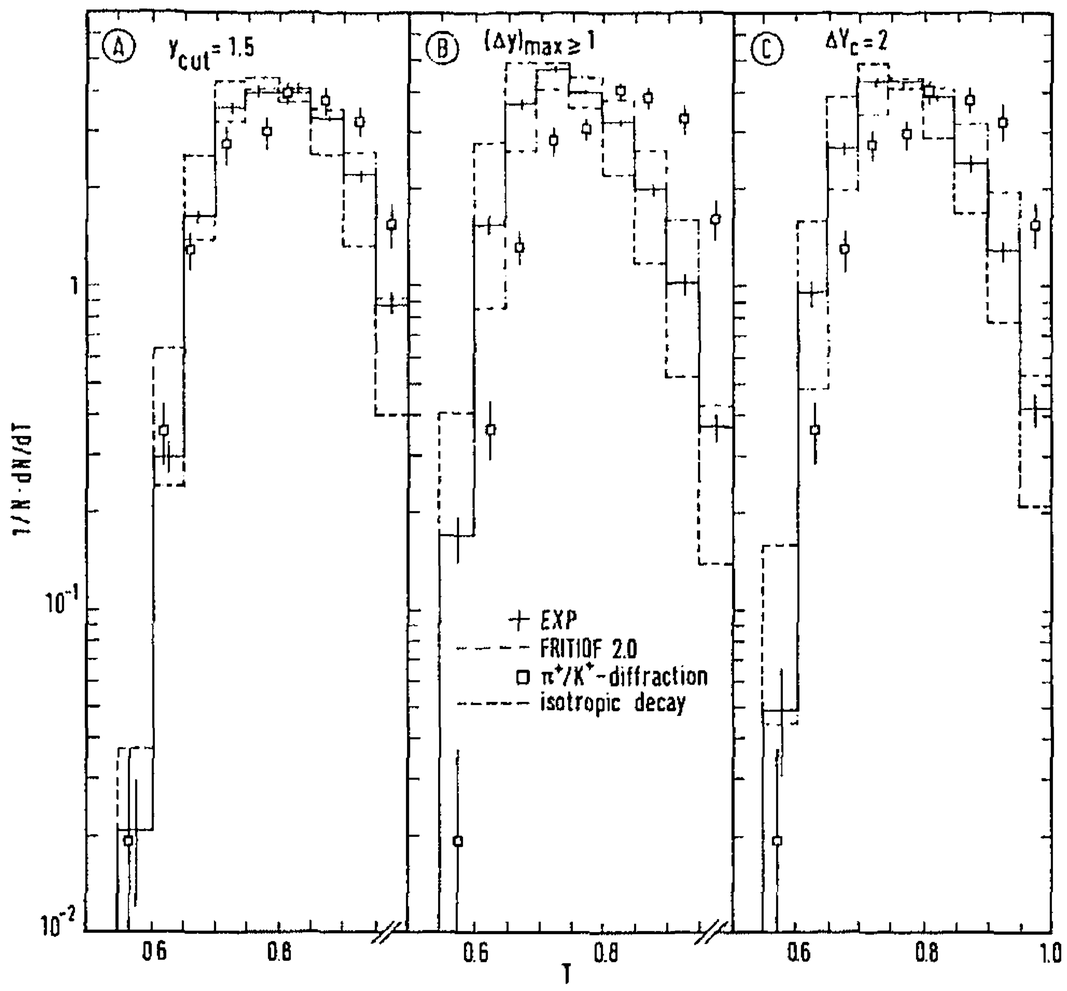

Fig. 8a–c. The thrust T-distribution for the leading cluster fragmentation for events with $n=n_{ch}+n_{neut}\geqq 4$ particles in the pion fragmentation region. The data on π^+/K^+-diffraction at 250 GeV/c [9] and isotropic decay predictions are also presented

[12] we consider that the leading hadron phenomenon is connected to valence quark transfer from the projectile to a secondary hadron. Thus, in $\pi^+ p$-collisions the leading hadron spectrum can be defined as the difference between the inclusive spectrum of positive (consisting for more than 90% of π^+'s in the beam fragmentation region [12]) and negative (consisting for $(93\pm 3)\%$ of π^-'s [12]) particles. One can extract from Fig. 1d that in the interval $0.2<x<0.92$ (where the central production and proton diffraction processes are small) the average value of the inelasticity is $\langle k_h\rangle=(1-\langle x_h\rangle)=0.56\pm 0.02$. Similar values of $\langle k_h\rangle$ are obtained in other experiments (see e.g. [18, 19]). Thus, the mean inelasticity obtained from the leading hadron spectrum is largely overestimated.

2) *The P_T^2-distribution* (Fig. 2) has an approximately exponential form with a slope b varying between 2.5 and 4.1 $(\mathrm{GeV/c})^{-2}$, according to the selection method chosen.

3) *The M^2_{eff}-distribution* (Fig. 3) agrees with that in single-diffractive processes [9] in the region of $2\leqq M^2_{\mathrm{eff}}\leqq 20\,(\mathrm{GeV/c^2})^2$ for methods II and III of cluster separation, but falls more steeply for method I. In all cases, predominantly low mass leading clusters are excited ($\langle M^2_{\mathrm{eff}}\rangle/s\leqq 0.01$).

Table 1. Mean values of the collective variables as indicated

Method	$\langle P_\parallel\rangle/p_{\mathrm{lab}}$	$\langle X\rangle$	$\langle P_T^2\rangle$ $(\mathrm{GeV/c})^2$	$\langle M^2_{\mathrm{eff}}\rangle$ $(\mathrm{GeV/c^2})^2$	$\langle t\rangle$ $(\mathrm{GeV/c})^2$	$\langle n_{\mathrm{ch}}\rangle$	$\langle Q\rangle$
I. $y_{\mathrm{cut}}=1$–2							
Exp	0.86–0.66	0.84–0.66	0.51–0.32	4.73–0.69	1.48–0.75	3.21–1.59	0.75–0.50
F2.0[a]	0.85–0.64	0.83–0.64	0.52–0.30	5.26–0.80	1.71–0.78	2.53–1.25	0.70–0.46
F_e2.0[b]	0.88–0.74	0.87–0.73	0.38–0.29	3.91–0.82	1.03–0.58	2.83–1.62	0.76–0.56
F3.0[c]	0.87–0.68	0.85–0.67	0.32–0.21	5.15–0.87	1.23–0.63	2.51–1.31	0.73–0.50
Lund	0.88–0.68	0.87–0.67	0.25–0.22	5.35–0.85	0.98–0.64	2.79–1.43	0.89–0.65
IIa. $(\Delta y)_{\mathrm{max}}$							
Exp	0.79±0.01	0.77±0.01	0.38±0.01	3.87±0.05	0.94±0.01	3.00±0.02	0.70±0.01
F2.0	0.77±0.01	0.75±0.01	0.39±0.01	4.35±0.03	1.03±0.01	2.22±0.01	0.65±0.01
F_e2.0	0.84±0.01	0.82±0.01	0.31±0.01	4.08±0.03	0.74±0.01	2.64±0.01	0.76±0.01
F3.0	0.80±0.01	0.77±0.01	0.25±0.01	4.32±0.03	0.71±0.01	2.17±0.01	0.68±0.01
Lund	0.75±0.01	0.73±0.01	0.19±0.01	4.30±0.04	0.52±0.01	2.20±0.02	0.76±0.01
IIb. $(\Delta y)_{\mathrm{max}}\geqq 1$							
Exp	0.82±0.01	0.81±0.01	0.37±0.01	4.22±0.05	0.91±0.01	3.15±0.02	0.74±0.01
F2.0	0.82±0.01	0.80±0.01	0.39±0.01	4.77±0.04	0.93±0.01	2.35±0.01	0.70±0.01
F_e2.0	0.85±0.01	0.84±0.01	0.30±0.01	4.19±0.04	0.71±0.01	2.69±0.01	0.78±0.01
F3.0	0.83±0.01	0.81±0.01	0.24±0.01	4.65±0.04	0.65±0.01	2.27±0.01	0.71±0.01
Lund	0.79±0.01	0.77±0.01	0.19±0.01	4.77±0.05	0.51±0.01	2.35±0.02	0.80±0.01
III. $\Delta Y_c=1.5$–2							
Exp	0.81–0.89	0.81–0.88	0.30–0.30	1.97–3.75	0.48–0.53	1.94–2.58	0.67–0.77
F2.0	0.83–0.92	0.83–0.91	0.29–0.27	2.60–4.57	0.55–0.44	1.75–2.14	0.64–0.79
F_e2.0	0.84–0.91	0.84–0.90	0.25–0.24	2.05–3.64	0.45–0.45	2.05–2.53	0.68–0.81
F3.0	0.84–0.91	0.83–0.90	0.18–0.17	2.55–4.30	0.38–0.30	1.73–2.07	0.67–0.82
Lund	0.80–0.88	0.79–0.87	0.18–0.18	2.33–4.36	0.40–0.35	1.78–2.21	0.79–0.89

[a] Fritiof 2.0; [b] Fritiof-eff 2.0; [c] Fritiof 3.0

Table 2. Mean values of the collective variables as indicated, for events with $n=(n_{ch}+n_{neut})\geqq 4$ particles in the pion fragmentation region

Method	$\langle T\rangle$	$\langle S\rangle$	$\langle\cos\theta_T\rangle$	$\langle\cos\theta_S\rangle$	$\langle Q_f\rangle$	$\langle Q_b\rangle$	$\langle Q_f Q_b\rangle$
I. $y_{cut}=1$–2							
Exp	0.78–0.83	0.40–0.30	0.49–0.32	0.49–0.32	0.44–0.25	0.30–0.23	–(0.68–0.43)
F 2.0[a]	0.79–0.83	0.37–0.31	0.50–0.34	0.51–0.33	0.41–0.30	0.29–0.23	–(0.44–0.38)
F_e 2.0[b]	0.80–0.84	0.36–0.30	0.52–0.35	0.53–0.36	0.47–0.28	0.26–0.36	–(0.63–0.51)
F 3.0[c]	0.79–0.83	0.38–0.32	0.51–0.33	0.52–0.33	0.41–0.31	0.31–0.23	–(0.47–0.42)
Lund	0.78–0.81	0.40–0.32	0.54–0.33	0.55–0.34	0.56–0.36	0.33–0.26	–(0.37–0.20)
IIa. $(\Delta y)_{max}$							
Exp	0.76±0.01	0.43±0.01	0.57±0.01	0.58±0.01	0.48±0.02	0.37±0.02	–0.94±0.03
F 2.0	0.78±0.01	0.39±0.01	0.57±0.01	0.57±0.01	0.46±0.01	0.37±0.01	–0.53±0.01
F_e 2.0	0.80±0.01	0.38±0.01	0.61±0.01	0.62±0.01	0.51±0.02	0.37±0.02	–0.70±0.02
F 3.0	0.78±0.01	0.39±0.01	0.57±0.01	0.58±0.01	0.46±0.01	0.37±0.01	–0.57±0.01
Lund	0.78±0.01	0.42±0.01	0.60±0.01	0.61±0.01	0.57±0.02	0.34±0.02	–0.50±0.02
IIb. $(\Delta y)_{max}\geqq 1$							
Exp	0.76±0.01	0.43±0.01	0.58±0.01	0.59±0.01	0.49±0.02	0.37±0.02	–0.95±0.03
F 2.0	0.78±0.01	0.40±0.01	0.58±0.01	0.60±0.01	0.47±0.01	0.37±0.01	–0.54±0.01
F_e 2.0	0.80±0.01	0.37±0.01	0.62±0.01	0.62±0.01	0.51±0.01	0.37±0.01	–0.70±0.01
F 3.0	0.78±0.01	0.40±0.01	0.58±0.01	0.59±0.01	0.46±0.01	0.38±0.01	–0.58±0.01
Lund	0.78±0.01	0.40±0.01	0.62±0.01	0.64±0.01	0.58±0.01	0.34±0.01	–0.51±0.01
III. $\Delta Y_c=1.5$–2							
Exp	0.78–0.78	0.40–0.40	0.47–0.60	0.48–0.61	0.41–0.48	0.35–0.36	–(0.77–0.83)
F 2.0	0.80–0.80	0.37–0.37	0.50–0.64	0.51–0.65	0.42–0.49	0.32–0.39	–(0.46–0.47)
F_e 2.0	0.81–0.81	0.35–0.36	0.48–0.63	0.48–0.64	0.48–0.53	0.31–0.35	–(0.66–0.66)
F 3.0	0.79–0.79	0.38–0.37	0.48–0.63	0.49–0.64	0.41–0.49	0.34–0.40	–(0.52–0.50)
Lund	0.79–0.79	0.40–0.39	0.48–0.62	0.50–0.65	0.52–0.59	0.35–0.39	–(0.36–0.41)

[a] Fritiof 2.0; [b] Fritiof-eff 2.0; [c] Fritiof 3.0

4) *The t-distribution* (Fig. 4) has an approximately exponential form with a slope b varying between 0.8 and 2.0 $(\mathrm{GeV/c})^{-2}$. This value is much smaller than generally observed for single-diffractive processes ($b_{diff}\approx 6$–$10\,(\mathrm{GeV/c})^{-2}$) [6]. Thus, experimental evidence is obtained that the non-single-diffractive process $hp\to H^*X$ is less peripheral than single-diffraction dissociation.

We have checked that the form of the distribution in t and P_T^2 does not depend strongly on the criteria of momentum balance (Sect. 2). In particular, when the restriction on the observed total transverse momentum $|p_T^{RCBC}+p_T^{EM}|$ is varied from 0.5 GeV/c to 0.1 GeV/c, the average values of P_T^2 and t decrease by (13–20)% and by (25–30)% respectively. The slope for t-distributions increases to (1.3–2.9)$(\mathrm{GeV/c})^{-2}$, still at least a factor two smaller than that of diffraction dissociation. The other quantities presented in Tables 1 and 2 do not change significantly.

5) *The charge multiplicity distribution* (Fig. 5b, c) has an excess at odd values for methods II and III. This can be interpreted as a reflection of the total *charge distribution* (Fig. 7), which has a sharp peak at charge $Q=+1$. The most probable value of the leading cluster charge is equal to the incident hadron charge. The events with $Q\neq 1$ correspond to the case when one or more comparatively slow fragmentation products of the leading cluster are not accepted by our methods or a charge exchange has taken place. This can lead to a value of average charge $\langle Q\rangle<1$.

6) For all three methods, *the M_{eff}-dependence of the average charge multiplicity* $\langle n_{ch}\rangle$ (Fig. 6) is stronger than in the diffractive process [9]. However, we shall show below (Sect. 4) that the essential part of this difference may be due to the restricted efficiency of neutral particle detection in our experiment. If this is taken into account the data for non-diffractive and diffractive processes disagree only in the comparatively high mass region ($M_{eff}>4$–$5\ \mathrm{GeV/c^2}$).

7) *The charge Q distribution* peaks at $Q=1$ (Fig. 7), weakest for method I, strongest for method III.

8) *The thrust distribution* (Fig. 8) is peaked at lower T values than in diffraction dissociation [9]. Nevertheless, the mean values of $\langle T\rangle\approx 0.76$–$0.83$ and $\langle S\rangle\approx 0.30$–$0.43$ indicate non-isotropy also for leading cluster fragmentation. The distributions expected for isotropic cluster decay (obtained by Monte-Carlo calculations using the experimentally observed cluster multiplicity distribution) do not agree with our data (see dashed histograms in Fig. 8).

The sphericity and thrust angle distributions are shifted towards angles larger than those of diffraction dissociation. The average value for $\cos\theta_T$ varies from 0.32 to 0.60 (Table 2), while for the single-diffractive process $\langle\cos\theta_T\rangle=0.72$ [9]. We have, furthermore, studied

the M_{eff}-dependence of the thrust and sphericity distributions and find that with increasing M_{eff} the jet-like structure of non-diffractive fragmentation becomes less pronounced. Particularly, for the rapidity gap method $(\Delta y)_{\max} \geqq 1$ in the mass regions $M_{\text{eff}} \leqq 2\,\text{GeV/c}^2$, $2 < M_{\text{eff}} < 4\,\text{GeV/c}^2$ and $M_{\text{eff}} \geqq 4\,\text{GeV/c}^2$ the average values of thrust and sphericity are $\langle T \rangle = 0.81, 0.77, 0.73$ and $\langle S \rangle = 0.35, 0.42, 0.57$, respectively.

9) The average charge of the forward jet, i.e. the charge in the forward hemisphere with respect to the total momentum of the fragmentation products, calculated in the rest frame of this system of particles, is $\langle Q_f \rangle = 0.45 \pm 0.04$ for methods II and III, i.e. close to the average charge of the π^+-meson valence quarks. The average charge of the backward jet is smaller (see Table 2) due to a loss of slow particles not accepted as fragmentation products. The forward and backward charges are strongly negatively correlated, the correlation moment varies from –0.42 to –1.00.

10) The average collective characteristics of the subsample with $Q = +1$ (not shown) are approximately the same as for the full sample.

We conclude that certain trends can indeed be observed in the collective characteristics of leading hadron clusters. These trends are common to all three selection methods applied. Noticeably different from the behaviour observed in diffraction dissociation are the dependence on four-momentum transfer and thrust.

4 Models

The experimental data are compared to the single-chain Lund [16] and the two-chain Fritiof 2.0 and Fritiof 3.0 [17] Monte-Carlo model predictions (for the definition of "Fritiof-eff" see below). Parameter values are default, except for the width of the Gaussian p_x and p_y transverse momentum distribution for primary hadrons (=0.44 GeV/c). The models, furthermore, include the production of tensor (besides pseudo-scalar and vector) mesons in the ratio PS:V:T = 50:35:15. Monte-Carlo events satisfying the "diffractive" criteria [12] are excluded. For the Fritiof 2.0 model the distribution and its average are presented in Figs. 1–8 and in Tables 1 and 2, while for the other two models only the average values are given.

As one can see from Figs. 1–8 and Tables 1–2, the qualitative agreement with the model predictions is satisfactory for the majority of the characteristics studied. As can be expected from the two-chain character of Fritiof, this model describes the data in general better than the old single-chain Lund model. The predictions of Fritiof 2.0 and Fritiof 3.0 differ strongly only for the distributions in P_T^2 and t. These are described noticeably better by Fritiof 2.0 (Figs. 2 and 4), evidently due to the fact that the primordial transverse momentum k_T of quarks within the incoming hadrons is included in Fritiof 2.0 but not in Fritiof 3.0. In the figures we, therefore, restrict ourselves to Fritiof 2.0.

The effect of the selection methods I–III is clearly seen in Fig. 1. The X spectrum becomes sharper at $X = 1$ as one goes from method I to III, both in data and model. In method I, the large momentum peak is wide, but slightly underestimated in size by the model. In methods II and III, the peak is wider in the data than in the model, even when taking into account $\langle \Delta p/p \rangle \sim 1.5\%$ in the data of that region. (Note that folding in the momentum resolution would amount to adding the content of the bin above $X \approx 1$ to that just below and therefore improve the agreement between the data and the model).

The model predictions for the M_{eff}^2 distribution (Fig. 3) are in qualitative agreement with the data for all three selection methods.

The charge multiplicity distributions (Fig. 5) of Fritiof peak at somewhat low values for all three methods. In methods II and III the odd-even effect in the data is, however, followed by the models. From Fig. 6 can be deduced that the shift to lower n_{ch} is present for all values of the mass of the leading cluster.

The differences between experimental data and model predictions can at least partly be connected to the restricted detection efficiency of neutral particles. This is 25–40% for π^0 (depending on x_{π^0}) [20] and about 40% for short-lived neutral strange particles [14] (long-lived neutral kaons and neutrons are not considered). Application of the selection criteria on total momentum balance (Sect. 2 above) leads to a suppression of events with a relatively large number of neutral particles or with large momentum of the neutrals.

In order to reveal the influence of the above bias we include the neutral particle detection efficiencies into the Fritiof Monte-Carlo predictions. The same selection criteria are applied to generated events as to the experimental ones. The results are shown by dot-dot-dashed lines in Fig. 6 and indicated "Fritiof-eff" in the Tables. One can see that the model predictions for $\langle n_{\text{ch}} \rangle$ increase by 20–30% as compared to the "non-distorted" Fritiof predictions and qualitatively describe the data. Note that the difference between these data and the diffraction dissociation data in the low mass region ($M_{\text{eff}} < 4\text{GeV}$) is approximately equal to this factor. So, for $M_{\text{eff}} < 4$ GeV our corrected data become compatible with the diffractive ones. However, for higher mass ($M_{\text{eff}} > 4$–5 GeV) the discrepancy between diffractive and non-diffractive data remains.

As for the influence of the neutral particle corrections on the other collective characteristics, the Fritiof-eff predictions describe the observed data not worse (in some cases better, e.g. $\langle n_{\text{ch}} \rangle$, $\langle Q \rangle$, $\langle Q_f Q_b \rangle$) than the Fritiof model. Exceptions are the P_T^2 and t distributions, for which the Fritiof-eff predictions are noticeably shifted towards smaller values.

The charge distribution (Fig. 7) qualitatively agrees with the Fritiof prediction. However, the probability for $Q = 1$ is slightly overestimated in the model relative to that in the experiment when methods I and III are applied.

The average characteristics $\langle T \rangle$, $\langle S \rangle$, $\langle Q_f \rangle$, $\langle Q_b \rangle$ of the jet-like structure in beam fragmentation are approximately reproduced by the Fritiof model (Table 2).

However, in Fritiof the T-distribution is somewhat shifted towards higher values (Fig. 8) and the forward-backward charge correlation $\langle Q_f Q_b \rangle$ is badly underestimated for all three methods (however Fritiof-eff somewhat improves the agreement for $\langle Q_f Q_b \rangle$).

5 Conclusions

Collective characteristics are studied of non-single-diffractive hadron systems produced in beam fragmentation of π^+ p-collisions at 250 GeV/c. It is shown that the pion fragmentation products carry on average a fraction of 0.8 ± 0.1 of the incident momentum, so that only 0.2 ± 0.1 of the incident momentum is spent for particle production in the central region. This value is considerably smaller than that deduced from leading hadron spectra. The momentum transfer distribution shows that the non-single-diffractive processes are less peripheral than the diffractive ones. The analysis of thrust and sphericity shows jet-like structure of pion fragmentation, but less prominent than in diffraction dissociation. The forward charge $\langle Q_f \rangle = 0.45 \pm 0.04$ agrees with the average charge of the beam valence quarks.

The Fritiof 2.0 model, which includes the primordial transverse momentum, qualitatively describes the experimental data.

Acknowledgements. It is a pleasure to thank the EHS coordinator L. Montanet and the operating crews and staffs of EHS, SPS and H2 beam, as well as the scanning and processing teams of our laboratories for their invaluable help with this experiment. We are grateful to III. Physikalisches Institut B, RWTH Aachen, Germany, for early contributions to this experiment.

References

1. R.C. Hwa: Phys. Rev. Lett. 52 (1984) 492
2. C.Y. Wong: Phys. Lett. 52 (1984) 1393
3. J. Hüfner, A. Klar: Phys. Lett. 145 B (1984) 167
4. L.P. Csernai, J.I. Kapusta: Phys. Rev. D 29 (1984) 2664; Phys. Rev. D 31 (1985) 2795
5. S. Daté, M. Gyulassy, H. Sumiyoshi: Phys. Rev. D 32 (1985) 619
6. K. Goulianos: Phys. Rep. 101 (1983) 169
7. A.M. Smith et al. R 608 Coll.: Phys. Lett. B 163 (1985) 267; Phys. Lett. B 167 (1986) 248
8. D. Bernard et al. UA 4 Coll.: Phys. Lett. B 166 (1986) 459
9. M. Adamus et al. NA 22 Coll.: Z. Phys. C – Particles and Fields 33 (1988) 301
10. M. Aguilar-Benitez et al.: Nucl. Instrum. Meth. 205 (1983) 79
11. M. Adamus et al. NA 22 Coll.: Z. Phys. C – Particles and Fields 32 (1986) 475
12. M. Adamus et al. NA 22 Coll.: Z. Phys. C – Particles and Fields 39 (1988) 311
13. I.V. Ajinenko et al. NA 22 Coll.: Z. Phys. C – Particles and Fields 35 (1987) 7
14. I.V. Ajinenko et al. NA 22 Coll.: Z. Phys. C – Particles and Fields 44 (1989) 573; I.V. Ajinenko et al. NA 22 Coll.: Z. Phys. C – Particles and Fields 46 (1990) 525
15. M.M. Aivazyan et al. NA 22 Coll.: Z. Phys. C – Particles and Fields 42 (1989) 377
16. B. Andersson, G. Gustafson, G. Ingelman, T. Sjöstrand: Phys. Rep. 97 (1983) 31
17. B. Andersson, G. Gustafson, B. Nilsson-Almqvist: Nucl. Phys. B 281 (1987) 289; Lund preprint TP 87-6
18. G.N. Fowler et al.: Phys. Rev. D 35 (1987) 870
19. V.S. Murzin, L.I. Saricheva: The physics of hadron processes, p. 184. Moscow: Energoizdat 1986
20. N.M. Agababyan et al. NA 22 Coll.: Z. Phys. C – Particles and Fields 41 (1989) 539